Study on the physical properties of a forest Glossic Retisol developed from loess in the Lublin Upland, SE Poland

Maja Bryk*

University of Life Sciences in Lublin, Institute of Soil Science and Environment Management, Leszczyńskiego 7, 20-069 Lublin, Poland

* PhD M. Bryk, maja.bryk@up.lublin.pl, ORCID iD: https://orcid.org/0000-0002-2291-1492

Abstract

Clay-illuvial soils with *argic* horizon and developed from loess or other silty deposits constitute high-quality arable land owing to favourable physical and chemical properties. There are thus numerous reports on such soils, considering their structure, compaction, erosion, water and air properties. However, there is still a lack of quantitative studies on structure and physical properties on analogous soils under forests. The aim of this research was therefore a comprehensive description of the physical state, including structure, water and air properties, of a forest Retisol developed from loess. Morphographic, morphological and morphometric parameters of structure, selected physicochemical and water and air properties and also relationships among the obtained parameters were analysed for genetic horizons O, Ah, AE, E, Bt/E, Bt, BtC and C. The field survey and soil structure images indicated that the studied forest soil had an undisturbed sequence of genetic horizons. The soil structure was shaped by soil flora and fauna causing bioturbation. Qualitative and quantitative structure analysis revealed that the O horizon had a loose arrangement, the Ah horizon had an aggregate crumb structure, the AE horizon had zones of an aggregate crumb structure and non-aggregate structure (fissured or with channels), while the remaining mineral horizons showed essentially a non-aggregate structure with varying proportions and sizes of planes and biogenic pores (i.e. cracked or fissured structure and structure with channels, respectively). The morphometric and physicochemical parameters facilitated a detailed analysis of the Retisol's physical state. The Retisol's structure type and degree of aggregate development directly influenced its hydraulic conductivity and water retention capacity. Therefore, under simulated precipitation, the soil water content and effective saturation varied mainly in the topsoil (O–E horizons) and virtually no changes were observed in the subsoil (Bt–C horizons). The research resulted in a comprehensive analysis of the physicochemical and morphometric parameters, their relationships, and structure images that were previously unavailable in other studies, covering the physical state of the entire pedon of a forest Retisol. The results obtained may serve, for example, as a reference (control) for analogous soils located in non-forest ecosystems and become an element in space-for-time substitution scenarios aimed at assessing the intensity of anthropogenic transformation.

1. Introduction

The dominant soil processes in Europe result from the conditions typical of humid continental (Dfb), oceanic (Cfb) and hot semi-arid (Bsh) climates (Soil Atlas of Europe, 2005; Beck et al., 2018). The climate of Poland is classified as continental with warm summer and no dry season (Dfb; Beck et al., 2018), with oceanic influences marked in the western part of the country, gradually weakening towards the east. The average annual temperature is 6–8.5°C and the average annual precipitation is 600 mm. As a result of a larger total precipitation than evaporation, the soils are dominated by leaching water regime. The primary vegetation in Poland consists of deciduous and mixed forests in rich habitats and coniferous forests in poorer environ-

ments (Gilewska, 1999). In line with the climatic conditions and vegetation, as well as owing to the considerable diversity of parent rocks, Poland has several types of zonal soils, with clay-illuvial ones prevailing. These soils developed from a variety of parent materials: loamy and sandy glacial deposits, silt (e.g. loess) and weathered rocks and slope deposits of loamy texture. Their pedogenesis often involved various processes in addition to the vertical translocation of clay particles by percolating water. As a result, the soils show a great diversity in their profile morphology (Kabała and Musztyfaga, 2015; Polish Soil Classification, 2019). The Polish Soil Classification (2019) identifies therefore 13 subtypes of clay-illuvial soils, which mostly correspond to Luvisols, Retisols, Luvic Planosols and Luvic Stagnosols according to the WRB (IUSS Working Group WRB, 2022).

1

Luvisols cover ca. 6% of Europe, mainly in the East European Plain and Central Europe but also in the Mediterranean region (Soil Atlas of Europe, 2005). In Poland, the clay-illuvial soils are common in both lowland and upland regions (e.g. Glina et al., 2013), estimated to account for at least 45% of the country (Polish Soil Classification, 2019). In southern Poland, the parent rocks of these soils are mainly loess and loess-like deposits (Słowińska-Jurkiewicz, 1989; Krupski et al., 2021). Under natural conditions, these soils are mostly covered with deciduous forests. However, owing to their favourable physical and chemical properties, the clay-illuvial soils developed from loess or other silty deposits are suitable for a wide range of agricultural purposes, constituting high-quality arable land. The high economic significance of these arable soils resulted in extensive research on topics such as their structure, compaction, erosion, water and air properties. For example, Toková et al. (2023) examined the effect of biochar on selected physical and hydrophysical soil properties of an arable silty loam Haplic Luvisol in Slovakia. Klíč et al. (2022) assessed the impact of land use (arable and forest) on the aggregate size distribution in a Haplic Luvisol developed on loess in Czechia during dry and wet sieving. Huang et al. (2022) used disturbed samples of the A horizon from an arable Stagnic Luvisol derived from loess (Germany) to investigate the influence of soil structure on deformation, pore water pressure and air permeability during compaction and subsequent shearing. Obalum et al. (2019) studied the effects of reduced tillage and organic matter on soil aggregate stability of an arable silt-loam Luvisol (Germany) through different aggregate stability tests.

However, there is still a lack of quantitative studies on the structure and other physical properties of analogous soils under forest vegetation. The aim of this research was therefore a comprehensive description of the physical state, including structure, water and air properties of a forest Retisol developed from loess. Specifically, the following analyses were conducted: (a) morphographic, morphological and morphometric analysis, which provided a qualitative description, interpretation and quantitative description of soil structure, respectively; (b) analysis of selected physicochemical properties; (c) analysis of selected water and air properties; and (d) analysis of relationships among the obtained parameters for all identified genetic horizons.

2. Materials and methods

2.1. Study area

The studied soil was located in SE Poland (physico-geographical subprovince 343 Lublin-Lviv Upland, macroregion 343.2 Roztocze Upland, mesoregion 343.21 Western Roztocze; Solon et al., 2018) near Albinów Duży (50°43'14.0" N, 22°44'27.5" E; 317 m a.s.l.), in the area covered by loess deposits ca. 7–10 m thick (Wągrowski, 1996). In the Western Roztocze, the mean annual temperature and precipitation are 7.4°C and 650 mm, respectively (Buraczyński, 2002). The soil pit was made at the summit of a hill, in an area of undulating (hilly) relief with denivelations over 2 km in the range of 10–75 m, in a mesophytic deciduous forest composed of oak *Quercus robur* and *Q. petraea*, hornbeam *Carpinus betulus* and lime *Tilia cordata* (plant community *Tilio cordatae-Carpinetum betuli* Tracz. 1962). The soil's profile was thoroughly examined and described in the field and the genetic horizons were identified (Fig. 1). The soil was classified as a clay-illuvial soil with tonguing in the *argic* horizon (PPzc; Polish Soil Classification, 2019) and an Epidystric Eutric Glossic Retisol (Pantosiltic, Cutanic, Differentic, Ochric) (RT-gs.eu.dyp-sle.ct.df. oh; IUSS Working Group WRB, 2022). The soil studied will be further referred to as the Retisol.

2.2. Soil physicochemical parameters

Soil samples were taken from the recognised genetic horizons (Table 1). Bulk samples of ca. 2 kg with disturbed structure were collected to determine soil's texture (SA, sand 0.05–2 mm; SI, silt 0.002–0.05 mm; CL, clay <0.002 mm fraction content, g g^{-1}, by a combination of the hydrometer and the wet-sieve methods; ISO 11277, 2009), total organic carbon (TOC, g (100 g)$^{-1}$; ISO 14235, 1998), pH in a 1:5 (v/v) suspension of soil in distilled water (ISO 10390, 2021), CaCO$_3$ content (ISO 10693, 1995) and particle density (PD, Mg m^{-3}; ISO 11508, 2017).

2.3. Soil air and water properties

Soil core samples with preserved structure were taken vertically in 12 replicates from each horizon into metal cylinders with a volume of 100 cm³. Six soil cores were used to determine soil bulk density (BD, Mg m^{-3} by the gravimetric method after drying at 105°C) and soil water retention curves (SWRCs). For the SWRCs, the soil samples were first saturated with water (soil water potential Ψ of 0 kPa). Next, measurements of soil water content were performed at Ψ of −1, −3, −10, −15, −30, −50, −150, −500 and −1500 kPa after stabilizing the samples on porous ceramic plates in the pressure chambers (Eijkelkamp, The Netherlands; SoilMoisture Equipment Co., USA). The volumetric soil water content (WC, cm³ cm^{-3}) was determined using the thermogravimetric method. Then, pore volume fractions were calculated using WC at each Ψ in the selected ranges of equivalent diameters (ED < 0.2, 0.2–0.6, 0.6–2, 2–6, 6–10, 10–20, 20–30, 30–100, 100–300, > 300 μm), where the equivalent diameters were evaluated from: ED = 300/|Ψ|.

The soil compactness was categorized according to the BD values as follows: very low, BD < 0.90 Mg m^{-3}; low, 0.91–1.10; medium-low, 1.11–1.30; medium, 1.31–1.50; medium-high, 1.51–1.70; high, 1.71–1.90; and very high, 1.91–2.10 (Święcicki et al., 1972). The total porosity of the soil (TP, cm³ cm^{-3}) was calculated using the PD and BD values.

Using the remaining six soil cores, saturated hydraulic conductivity (Ks, cm d^{-1}) was measured with the ICW laboratory permeameter (Eijkelkamp, The Netherlands). The Ks values were categorised as follows: <10.0, very low; 10.1–50.0, low; 50.1–200.0, medium; 200.1–1000, high; and >1000 cm d^{-1}, very high (Paluszek, 2011). The SWRCs were fitted to the means of the observed water retention data (WC at Ψ from −1 to −1500 kPa) using the RETC computer program (RETC 6.02; van Genuchten et al., 1991). Subsequently, the unsaturated

Table 1.
Chemical and physical properties of the Retisol. Different letters in a row indicate significant differences (P < 0.05) among horizons.

Horizon	O	Ah	AE	E	Bt/E	Bt	BtC	C
Depth, cm	0–5/7	5/7–15/22	15/22–35/47	35/47–50	50–95	95–145	145–170	> 170
Sampling depth, cm	0–5*, 0–8**	8–16	22–30	42–50	80–88	96–104	152–160	176–184
Munsell colour, moist	10YR 2/3	10YR 2/2	10YR 4/2	10YR 5/2		10YR 4/6	10YR 5/4	10YR 5/4
Munsell colour, dry	10YR 5/3	10YR 5/2	10YR 6/2	10YR 7/2		10YR 6/4	10YR 6/4	10YR 7/4
TOC, g (100 g)⁻¹	25.92	3.04	0.64	0.38	0.38	0.16	0.18	0.24
pH_{H2O}	5.33	5.80	4.90	4.99	5.50	5.75	5.96	5.81
PD, Mg m⁻³	1.89	2.40	2.63	2.67	2.67	2.69	2.68	2.69
BD, Mg m⁻³	0.64 ± 0.09 d	0.73 ± 0.21 d	1.23 ± 0.07 c	1.56 ± 0.04 ab	1.50 ± 0.13 b	1.58 ± 0.05 ab	1.59 ± 0.04 a	1.51 ± 0.04 b
Texture	n.a.	SiL	Si	SiL	SiL	SiL	SiL	SiL
SA, g g⁻¹	n.a.	0.29	0.12	0.15	0.15	0.18	0.17	0.17
SI, g g⁻¹	n.a.	0.65	0.80	0.79	0.79	0.56	0.63	0.66
CL, g g⁻¹	n.a.	0.06	0.08	0.06	0.06	0.26	0.20	0.17
TP, cm³ cm⁻³	0.661	0.696	0.532	0.416	0.438	0.413	0.407	0.439
MWC, cm³ cm⁻³	0.674 ± 0.064 a	0.664 ± 0.050 a	0.493 ± 0.021 b	0.447 ± 0.019 c	0.435 ± 0.020 c	0.436 ± 0.012 c	0.434 ± 0.015 c	0.445 ± 0.009 c
Ks, cm d⁻¹	13899.53 a	301.30 b	19.953 c	0.538 d	0.112 d	0.112 d	0.190 d	0.895 d
logKs	4.143 ± 0.628 a	2.479 ± 0.851 b	1.300 ± 0.374 c	-0.269 ± 1.058 d	-0.951 ± 0 d	-0.951 ± 0 d	-0.722 ± 0.560 d	-0.048 ± 0.995 d
AA, cm² cm⁻²	0.527 ± 0.055 a	0.260 ± 0.025 b	0.073 ± 0.013 d	0.102 ± 0.017 c	0.050 ± 0.030 e	0.045 ± 0.017 e	0.046 ± 0.011 e	0.044 ± 0.008 e
LA, cm cm⁻²	40.057 ± 2.219 a	28.798 ± 4.726 b	15.230 ± 3.134 c	8.726 ± 1.506 d	6.005 ± 1.090 e	6.925 ± 1.426 e	7.048 ± 1.141 e	6.001 ± 0.952 e
Np	12718 ± 4328 b	21667 ± 5356 a	22341 ± 5984 a	7799 ± 2633 cde	6151 ± 787 e	9672 ± 2719 bc	8557 ± 2634 bcd	6662 ± 915 de
NAp, cm⁻²	203.0 ± 69.9 b	358.0 ± 59.8 a	346.0 ± 94.0 a	119.0 ± 42.4 cde	95.7 ± 12.7 e	148.0 ± 42.2 bc	131.0 ± 40.5 bcd	101.0 ± 14.2 de
Np100	1160 ± 425 abc	1699 ± 596 a	1399 ± 199 a	676 ± 159 c	621 ± 88 c	790 ± 232 bc	1103 ± 282 ab	993 ± 208 b
NAp100, cm⁻²	18.5 ± 6.8 abc	27.9 ± 7.9 a	21.6 ± 3.2 ab	10.3 ± 2.3 e	9.7 ± 1.4 e	12.0 ± 3.5 de	16.9 ± 4.2 bc	15.1 ± 3.2 cd
Ns	13350 ± 1733 a	4010 ± 1057 b	755 ± 203 c	737 ± 183 c	393 ± 224 d	322 ± 122 d	263 ± 64 d	237 ± 81 d
NAs, cm⁻²	213.0 ± 27.7 a	66.6 ± 16.3 b	11.7 ± 3.1 c	11.2 ± 2.8 c	6.1 ± 3.5 d	4.9 ± 1.9 de	4.0 ± 1.0 de	3.6 ± 1.2 e
ANp, mm²	0.319 ± 0.156 a	0.080 ± 0.019 b	0.022 ± 0.004 d	0.098 ± 0.040 c	0.054 ± 0.034 c	0.032 ± 0.013 c	0.038 ± 0.012 c	0.044 ± 0.007 c
ANs, mm²	0.244 ± 0.058 e	1.295 ± 0.419 d	9.383 ± 2.685 c	9.320 ± 2.294 c	21.158 ± 9.210 b	24.108 ± 8.103 ab	27.509 ± 6.262 ab	33.359 ± 13.760 a

Explanations: TOC, total organic carbon; PD, particle density; BD, bulk density; SA, sand fraction; SI, silt fraction; CL, clay fraction; TP, total porosity; MWC, maximum water content; Ks, saturated hydraulic conductivity–geometric mean; AA, porosity; LA, relative length of pore–solid phase boundary; Np, number of pore cross-sections; NAp, relative number of pore cross-sections; Ns, number of solid phase element cross-sections; NAs, relative number of solid phase element cross-sections; Np100, number of pore cross-sections of area > 100 pix²; NAp100, relative number of pore cross-sections of area > 100 pix²; ANp, mean area of pore cross-section; ANs, mean area of solid phase element cross-section; * bulk and core samples, ** samples for structure analysis

hydraulic conductivity function was predicted using the geometric means of K_s and a dual-porosity Durner-Mualem model (Durner, 1994). RETC was run with the following fitting parameters: RWC (residual water content, $cm^3\,cm^{-3}$), α1, α2, $n1$, $n2$ and $l = 0.5$. The parameter $w2$ was gradually adjusted to maximise R^2 for regression of observed vs. fitted values (Table 2). Subsequently, the SWRC parameters obtained were incorporated into the input data for water flow simulations using HYDRUS-1D (version 4.17.0140) (Šimůnek et al., 1998, 2018). The α, n and l parameters in HYDRUS-1D are considered to be empirical coefficients affecting the shape of the hydraulic functions.

HYDRUS-1D was set to simulate the water flow in an eight-layer pedon of 200 cm depth over a 31-day period. The simulation employed a dual-porosity soil hydraulic model without hysteresis. Time-variable atmospheric boundary conditions were specified based on weather data at Frampol, with a surface water layer h up to 3 cm and free drainage. Evaporation

was neglected to focus on the impact of rainfall. For the purpose of the simulation, we applied weather data recorded during July 2011 at Frampol weather station (No. 250220080, located at 50°40' N, 22°40' E) of the Institute of Meteorology and Water Management–National Research Institute (IMGW–PIB) in Poland (IMGW–PIB, 2023). July 2011 was exceptionally wet with precipitation of 262.5 mm, which was three times higher than the 1991–2020 climatological standard normals for this area of Poland. The data obtained from IMGW–PIB were processed to fit the format requirements of HYDRUS-1D.

2.4. Soil structure

For the analysis of soil structure, samples with preserved structure were taken in two replicates in the vertical plane into metal boxes of 8 cm × 9 cm × 4 cm from the identified horizons (Fig. 1). The dried samples were impregnated with a polyes-

Table 2.
Parameters of the fitted soil water characteristic curves.

Parameter	O	Ah	AE	E	Bt/E	Bt	BtC	C
Residual water content, RWC, $cm^3\,cm^{-3}$	0.084	0.169	0.046	0.006	0.009	0.009	0.037	0.001
Saturated water content, MWC, $cm^3\,cm^{-3}$	0.674	0.664	0.493	0.447	0.435	0.436	0.434	0.445
α1, cm^{-1}	0.058	0.115	0.001	2.070	1.108	1.075	0.271	0.294
α2, cm^{-1}	0.283	0.002	0.122	0.001	0.001	0.001	0.001	0.001
$n1$	1.067	2.328	4.030	1.052	1.074	1.070	1.128	1.128
$n2$	1.786	2.190	1.393	2.193	5.020	3.748	5.658	5.157
$w2$	0.45	0.50	0.39	0.22	0.37	0.38	0.47	0.44
R^2	0.991	0.993	0.999	0.996	0.999	0.999	1.000	0.999

Explanations: RWC, residual water content; MWC, maximum (saturated) water content; α1, α2, $n1$, $n2$, $w2$, fitting parameters; R^2, coefficient of regression of observed vs. fitted values of SWRC
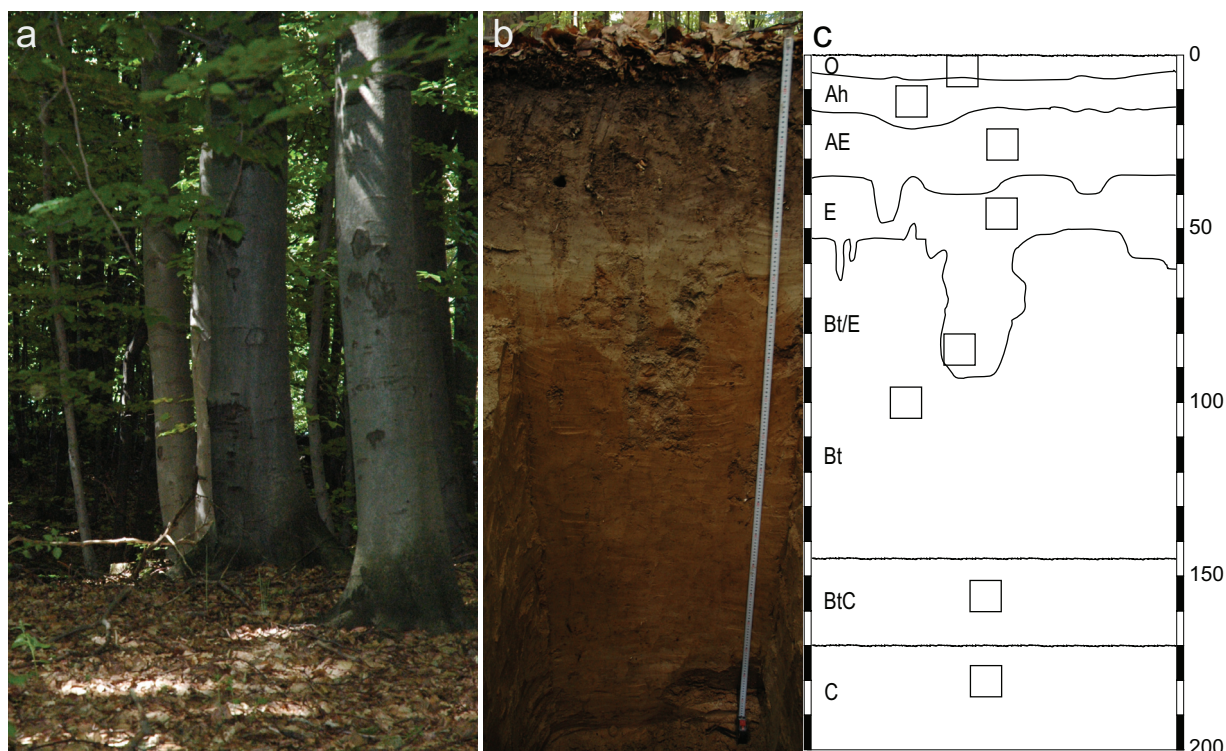
Fig. 1. (a) Vegetation at the study area, (b) photograph and (c) scheme of the Retisol's profile. Rectangles show sampling locations.

ter resin solution and after hardening cut and polished into slices of ca. 8 cm × 9 cm × 1 cm according to the methodology described earlier (Słowińska-Jurkiewicz et al. 2012; Bryk and Kołodziej, 2014; Bryk, 2016). In that manner, five (O) to eight (Ah–C) polished block faces were obtained. The specimen faces were scanned using an Epson Perfection 1200 Photo scanner with a resolution of 1200 × 1200 dpi and 24-bit colour depth, resulting in each image having ca. 4000 × 4000 pixels. Morphological structure analysis was carried out based on the soil blocks and their enlarged photos. The structure was described using the terminology proposed by Słowińska-Jurkiewicz et al. (2012), which incorporated the concepts of Brewer and Sleeman (1960), Beckmann and Geyger (1967), Jongerius and Rutherford (1979), FitzPatrick (1984) and Aguilar et al. (2023).

For morphometric analysis of structure, the scanned images were processed as previously specified (Bryk and Kołodziej, 2014). Then, morphometric parameters were measured for cross-sections of pores and solid phase elements detected in the obtained binary images. Due to the scanning resolution, the minimum diameter of the measured object was 21.17 μm. Using data from the entire image, the cross-sectional areas Api and Asi (cm^2) were measured for the pores and solid phase elements, respectively. Equivalent diameters were subsequently calculated as: EDp = 2(Api/π)$^{0.5}$ or EDs = 2(Asi/π)$^{0.5}$. The number (Np, Ns), Feret's diameters at 12 angles from 0 to 165° (DMAXpi and perpendicular to them DMINpi, cm) and perimeters (Lpi and Lsi, cm) of the pore and solid phase element cross-sections, on the other hand, were determined for cross-sections with centroids located within a protective frame which included the centrally-placed rectangular covering 90.25% of the area of each image. The entire areas of the images (*A*, cm^2) and the protective-frame areas for each image (*Af* = 0.9025*A*, cm^2) were then evaluated. In the following, these will be referred to as the sample area.

The following parameters were calculated for each Retisol's horizon by averaging the results obtained from relevant images:
–   the relative area of pore cross-sections (porosity, cm^2 cm^{-2}), AA = ΣApi/*A*;
–   the relative length of pore cross-sections' perimeter (the relative length of the boundary between the pore and solid phase cross-sections, cm cm^{-2}), LA = ΣLpi/*Af*;
–   the number of pore cross-sections per 1 cm^2 of the sample area (the relative number of pore cross-sections, cm^{-2}), NAp = Np/*Af*;
–   the number of solid phase element cross-sections per 1 cm^2 of the sample area (the relative number of solid phase element cross-sections, cm^{-2}), NAs = Ns/*Af*;
–   the mean area of pore cross-section (mm^2), ANp = ΣApi/Np;
–   the mean area of solid phase element cross-section (mm^2), ANs = ΣAsi/Ns.

The obtained morphometric parameters of the Retisol's structure were classified as follows:
–   AA: 0.000–0.100 very low, 0.101–0.200 low, 0.201–0.300 medium, 0.301–0.400 high and ≥ 0.401 cm^2 cm^{-2} very high;
–   ANp: 0.000–0.100 very small, 0.101–0.200 small, 0.201–0.300 medium, 0.301–0.400 large and ≥ 0.401 mm^2 very large;

–   ANs: 0.000–0.400 very small, 0.401–2.000 small, 2.001–10.000 medium, 10.001–50.000 large and ≥ 50.001 mm^2 very large;
–   LA: 0.000–10.000 very low, 10.001–20.000 low, 20.001–30.000 medium, 30.001–40.000 high and ≥ 40.001 cm cm^{-2} very high;
–   NAp: 0–100 very low, 101–200 low, 201–300 medium, 301–400 high and ≥ 401 cm^{-2} very high;
–   NAs: 0–50 very low, 51–100 low, 101–150 medium, 151–200 high and ≥ 201 cm^{-2} very high.

Moreover, elongation indices were calculated for the pore cross-sections of area larger than 100 pix^2 (0.045 mm^2) as: ELGp = = (DMAXpi – DMINpi) / (DMAXpi + DMINpi). The elongation index starts at 0 and reaches 1 for elongated shapes, where DMAX ≫ ≫ DMIN (Kołodziej et al., 2004). The pore cross-sections were classified based on the ELGp values: 0–0.2, 0.21–0.4, 0.41–0.6, 0.6–0.8 and > 0.8. For each class, the relative areas of pore cross-sections were calculated, ELGp1, ELGp2, ELGp3, ELGp4 and ELGp5, respectively. Subsequently, for the pore cross-sections of ELGp > 0.2 (Bryk et al., 2005) there were calculated the relative areas of horizontally (HORp), diagonally (DIAGp) and vertically (VERp) oriented pores. The pore orientation was categorised by the angle of the main axis (DMAXpi), where a horizontal orientation was 0°, diagonal included 15, 30, 45, 135, 150 and 165°, and vertical orientation included 60, 75, 90, 105 and 120°.

According to the laws of stereology (Russ and Dehoff, 2000), all calculated relative areas of the pore cross-sections (AA, ELGp1–ELGp2, HORp, DIAGp and VERp) represent the relative volume of the pores, i.e. porosity. Porosities in selected ranges of equivalent diameters (EDp < 100, 100–300, 300–1000, 1000–3000, > 3000 μm; classes AAp1–AAp5, respectively) and volume fractions of solid phase elements in selected ranges of equivalent diameters (EDs < 100, 100–300, 300–500, 500–1000, 1000–3000, 3000–10000, 10000–30000, > 30000 μm) were also calculated.

2.5. Statistical analysis

Soil physical and chemical parameters were tested for homogeneity of variance using the Levene's test and for normality using the Shapiro-Wilk normality test prior to ANOVA. The assumptions for ANOVA were not met, therefore differences among parameters for the Retisol's horizons were checked using the Kruskal-Wallis rank sum test followed by pairwise comparisons using the Wilcoxon rank sum test (P < 0.05) with P-value adjustment method of Benjamini and Hochberg (1995). Mean values and standard deviations were calculated for the studied parameters. Principal component analysis (PCA) was performed to examine relationships among the studied parameters in the Retisol's horizons. Then, Pearson's linear correlation coefficients were calculated for the selected variables based on the PCA results. Considering the number of analysed pairs of observations (n = 8), the correlations were statistically significant at P < 0.05 when R = |0.7068|. Nevertheless, only the strongest correlations were discussed, with R > |0.9|. The statistical analyses were conducted using Microsoft Excel and the R software environment (R Core Team, 2022) with the "factoextra" (Kassambara and Mundt, 2020), "FactoMineR" (Le et al., 2008) and "car" (Fox and Weisberg, 2019) packages.

5

3. Results

3.1. Physicochemical properties

The mineral part of the soil had a silt texture in the AE horizon and silt loam texture in other horizons (Table 1). Due to the migration of clay, the Ah, AE and E horizons showed lower clay content relative to the loess parent material C (0.06–0.08 g g^{-1} vs. 0.17 g g^{-1}). Illuviation led to accumulation of clay minerals in the Bt and BtC horizons, resulting in clay contents of 0.26 and 0.20 g g^{-1}, respectively.

The O and Ah horizons were characterised by a very low bulk density (BD) of 0.64–0.73 Mg m^{-3}. BD increased with depth to medium-low of 1.23 Mg m^{-3} in AE and medium-high of 1.50–1.59 Mg m^{-3} in E, Bt/E, Bt, BtC and C. The total porosity (TP) followed the opposite trend, with higher values in O and Ah, > 0.661 cm^3 cm^{-3}, medium in AE, 0.532 cm^3 cm^{-3}, and lower in the remaining horizons, < 0.439 cm^3 cm^{-3}.

Carbonates were not detected in the soil. The Retisol was acidic, with pH$_{water}$ ranging from 4.90 (AE) to 5.96 (BtC). The soil organic carbon content (TOC) decreased gradually with depth. TOC reached > 20 g (100 g)$^{-1}$ in the organic horizon, ca. 3 g (100 g)$^{-1}$ in the Ah horizon and 0.18–0.64 g (100 g)$^{-1}$ in the other soil horizons. The TOC content was affected by bioturbation which occurred with different degrees of intensity across the pedon. The main factors influencing soil faunal activity and root development were soil bulk density and clay content. In the more compacted Bt and BtC horizons, soil faunal activity was reduced and root growth was impeded. Consequently, less organic material was transferred to those horizons, leading to lower TOC compared to the E and C horizons (Table 1, Fig. 2).

3.2. Morphological description of macrostructure

The organic O horizon consisted of Oi and Oe subhorizons which were formed of loosely arranged beech leaves and oth-
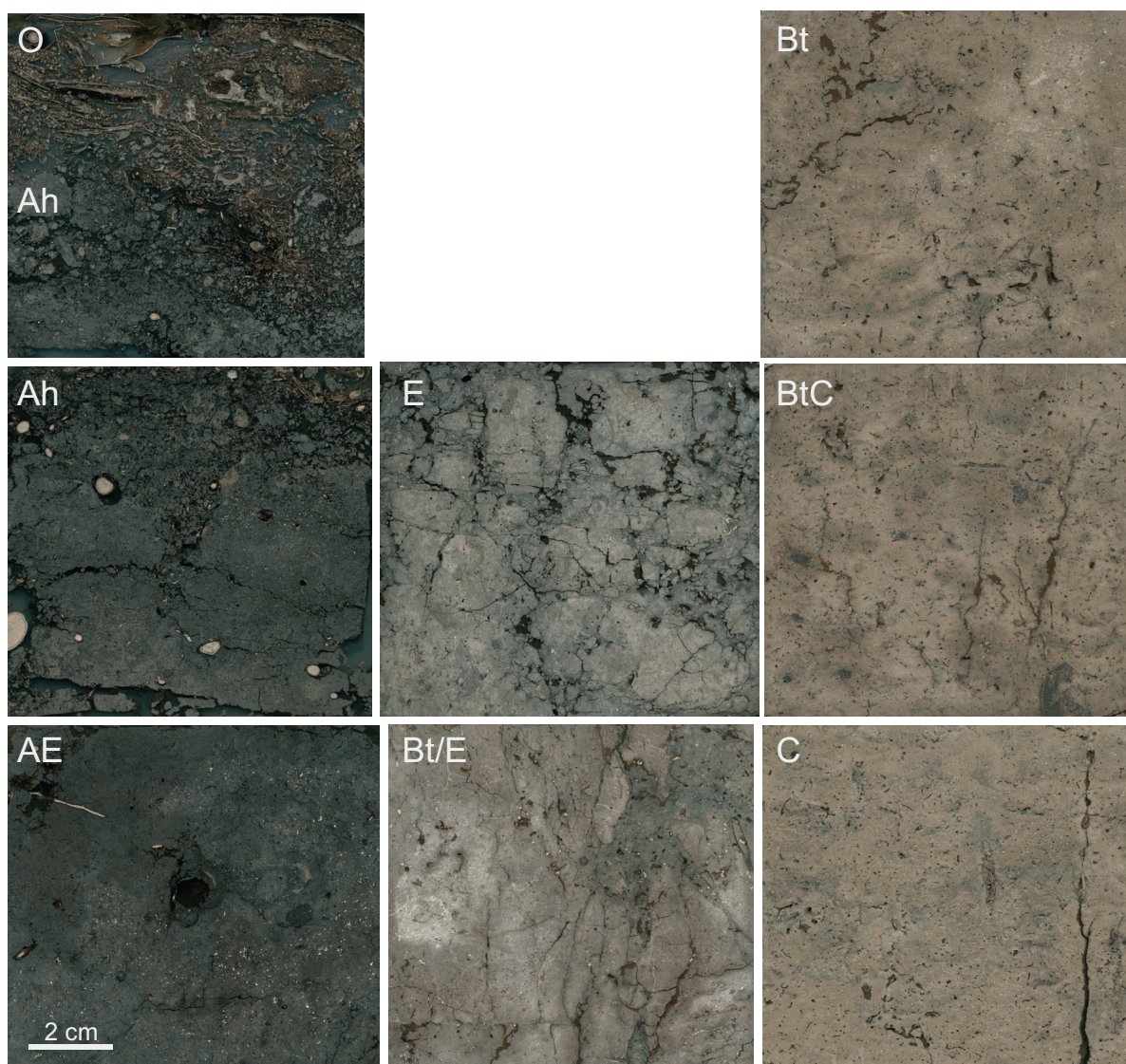
Fig. 2. Representative photographs of the Retisol's structure in the studied horizons: O-Ah, 0–8 cm; Ah, 8–16 cm; AE, 22–30 cm; E, 42–50 cm; Bt/E, 80–88 cm; Bt, 96–104 cm; BtC, 152–160 cm; C, 176–184 cm.

er plant debris, respectively (Fig. 2). An aggregate structure was evident in the Ah horizon, with strongly- to weakly-developed biogenic crumbs, loosely distributed in continuous pore space. However, in many zones, the crumbs were closely situated, revealing a non-aggregate structure with numerous, sometimes wide, biogenic channels that were created by plant roots and soil fauna. Some channels were filled with plant roots. The soil in the most compacted zones had a non-aggregate fissured structure, with the soil mass separated by long, horizontal, parallel pores (planes) of varying width, often interconnected. In the Ah horizon, numerous sections of fine roots were also visible. The AE horizon showed a similar structure to that in the lower part of the Ah horizon, with weakly-developed crumbs or without aggregates. In zones of intense soil faunal activity, an aggregate structure with strongly-developed crumbs was identified. Zoogenic channels reached a diameter of 10 mm and numerous cross-sections of fine roots were also visible. The structure of the E and Bt/E horizons was influenced by clay eluviation and bioturbation. In the vicinity of the roots, the soil showed an aggregate structure with sub-angular blocks up to 25 mm in size. Dark-coloured zones, created by megafauna, were also evident; they had a crumb structure and a structure with zoogenic channels. In zones of higher density, a cracked and fissured structure was present, with interconnecting planes of different directions. The lightest zones lacking humus were the most compacted and showed a non-aggregate cracked structure with narrow planes and small vughs (*Nadelstichporen*). The soil in the Bt horizon was much more compacted than in the overlying horizons and revealed mostly a non-aggregate structure with vughs. However, there were discernible wide channels created by megafauna and filled with humus material from the upper soil layers. Narrow planes branched off from the channels. Further analysis of bulk soil collected from the Bt horizon revealed numerous pores filled with clay along with clay coatings present on the pore walls. The BtC horizon had a structure with vertical and horizontal channels, filled with humus-rich material, and also zones of an aggregate structure with weakly- to moderately-developed crumbs. This was indicative of stronger bioturbation compared to the more compacted Bt horizon. In the parent material (the C horizon), a non-aggregate structure predominated, with fine vughs typical of loess. Nevertheless, even at this depth, the impact of animal activity was apparent as dark patches containing humus transported from the upper soil layers.

3.3. Morphometric description of macrostructure

As a consequence of the observed soil structure, the O and Ah horizons showed considerably higher porosity (AA) than the remaining part of the pedon. AA in the O horizon was very high and twice that of Ah, for which a medium AA was recorded (Table 1). The E horizon revealed a low AA and the other horizons – a very low AA of ca. 0.5 cm^2 cm^{-2}. The values of the relative length of pore cross-sections' perimeter (LA) in the four upper horizons progressively decreased with depth from very high to low with horizons O, Ah, AE and E statistically different from

each other and from lower horizons. In the remaining part of the pedon, LA was comparable and very low. The relative number of pore cross-sections (NAp) was high in the Ah and AE horizons, medium in O, low in E, Bt, BtC and C and very low in Bt/E. The relative number of solid phase element cross-sections (NAs) decreased gradually downwards in the Retisol's pedon, reaching very high values in O, low in Ah and very low in the underlying horizons. The measured porosity and number of pore cross-sections resulted in a large ANp in the O horizon and a very small ANp in the rest of the pedon. ANp showed statistical variation among the O, Ah, AE and E horizons but was comparable in size from the Bt/E horizon downwards. The mean area of solid phase element cross-section (ANs) gradually increased with depth, starting with very small values in O, through small ones in Ah, medium ones in AE and E and reaching very large values in lower horizons.

3.4. Size distribution of pores and solid phase elements

Size distributions of pores and solid phase elements measured by SWRC and image analysis (IA) are presented in Fig. 3. The O and Ah horizons were distinct from the rest of the soil, having the highest rate of macropores (MA, > 30 μm) as shown by both SWRCs and IA. In the other horizons, the volume of macropores was 2–3 times lower. The volume of mesopores (ME, 2–30 μm) obtained from the SWRCs varied in the Retisol's pedon. It was lower in the O and E horizons, medium in Ah, Bt/E, Bt, BtC and C, and higher in AE. The highest volume of micropores (MI, < 2 μm) was found in the O horizon and MI decreased progressively in the E, Ah, Bt/E, Bt, BtC, C and AE horizons. The Bt/E, Bt and BtC horizons had comparable differential porosities as measured by SWRC.

The image analysis allowed also for the assessment of the size distribution of solid phase elements. Once again, the O and Ah horizons were different from the rest of the pedon. These results were in line with the morphological analysis of macrostructure which identified an aggregate structure in the upper part of the Retisol. In the O horizon, both smaller (0.1–1 mm) and larger (> 1 mm) solid phase elements were visible. In the Ah horizon, elements of 1–30 mm in size were still discernible, although large cross-sections of solid phase elements, > 30 mm, predominated. The underlying horizons exhibited comparable arrangement of the solid phase, mostly consisting of elements larger than 30 mm, resulting in a continuous solid phase.

3.5. Shape and orientation of pore cross-sections

An analysis of shape and orientation of the pore cross-sections was carried out to support the interpretation of soil hydraulic conductivity. The largest volume of elongated pores was detected in the Ah horizon, 0.2093 cm^2 cm^{-2} (Table 3). More than twice as much elongated pores were found in the O and E horizons. The remaining horizons had only ca. 0.021–0.034 cm^2 cm^{-2} of such pores. In the next step, the orientation was determined for the elongated pores, i.e. belonging to classes ELGp2–ELGp5. As stated above, the cross-sections were
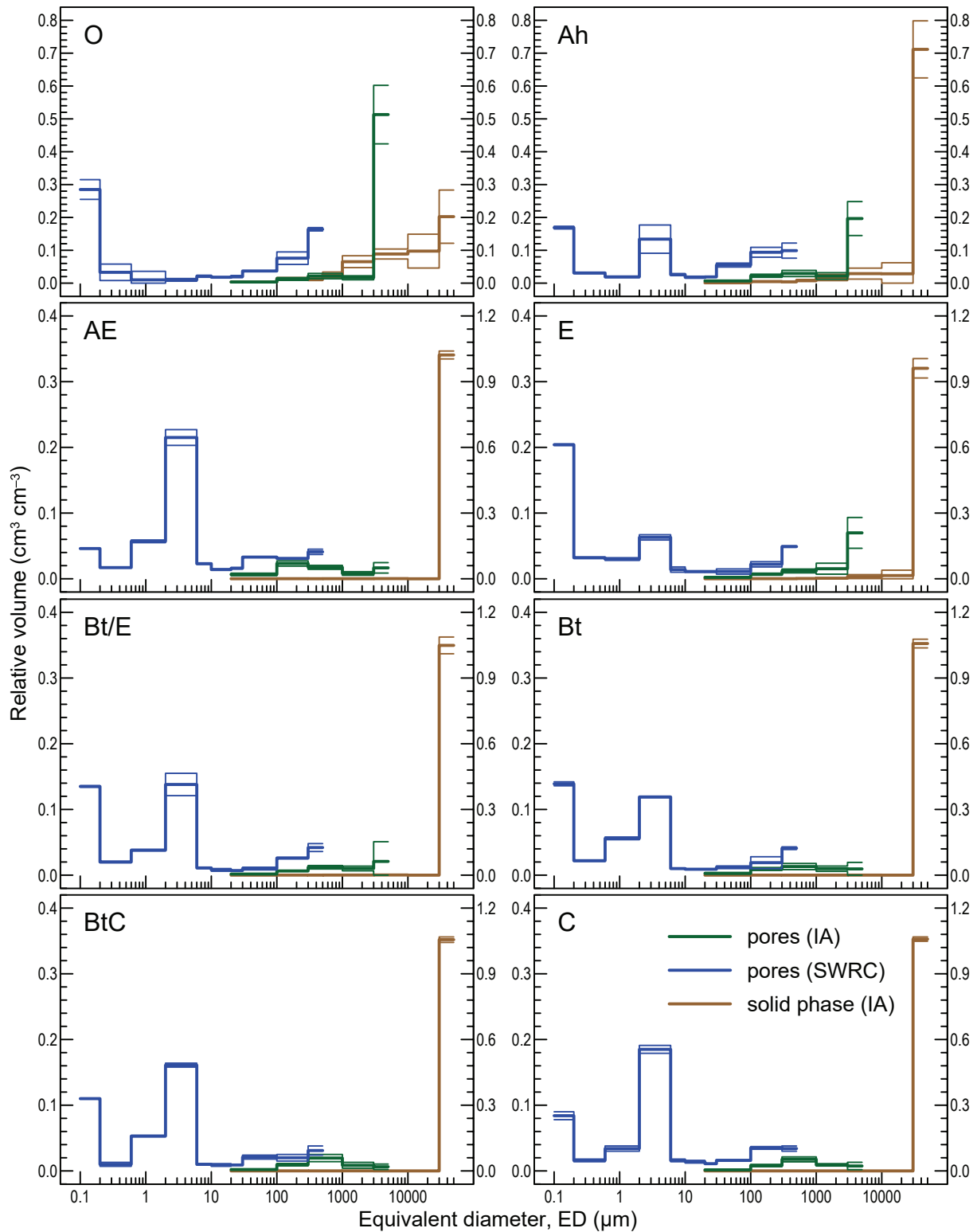
Fig. 3. Pore size distributions obtained from SWRC and image analysis (left axis) and solid phase element size distribution by image analysis (right axis) in the Retisol's horizons; thick line: mean value, thin line: ± standard deviation.

grouped based on their orientation into: horizontal pores (HORp) determining the transportation of substances mostly within a layer, and diagonal (DIAGp) with vertical (VERp) governing the movement of water both within and between the layers. Owing to their similar functionality and on the basis of

the preliminary statistical evaluation, the diagonal and vertical pores were combined into the DIVEp class. The highest volume of diagonal and vertical pores (DIVEp = DIAGp + VERp) was detected in the Ah horizon, 0.1779 cm^2 cm^{-2} (Table 3). Almost three times less such pores were detected in the O and E horizons, ca.

Table 3.
Relative area of pore cross-sections (cm^2 cm^{-2}) in the classes of elongation index (ELGp1–ELGp5) and classes of orientation (HORp, DIAGp and VERp) for pore cross-sections > 100 pix^2.

Parameter	O	Ah	AE	E	Bt/E	Bt	BtC	C
ELGp1	0.4779	0.0410	0.0181	0.0244	0.0110	0.0139	0.0112	0.0100
ELGp2	0.0255	0.1663	0.0176	0.0529	0.0154	0.0143	0.0155	0.0148
ELGp3	0.0488	0.0375	0.0099	0.0191	0.0144	0.0062	0.0095	0.0082
ELGp4	0.0028	0.0055	0.0023	0.0026	0.0040	0.0007	0.0018	0.0031
ELGp5	0.0000	0.0000	0.0000	0.0001	0.0001	0.0000	0.0000	0.0009
ELGp2_5	0.0771	0.2093	0.0298	0.0747	0.0339	0.0212	0.0268	0.0270
HORp	0.0127	0.0314	0.0038	0.0090	0.0042	0.0036	0.0046	0.0064
DIAGp	0.0429	0.1157	0.0152	0.0362	0.0161	0.0113	0.0142	0.0146
VERp	0.0215	0.0622	0.0108	0.0296	0.0135	0.0063	0.0080	0.0060
DIVEp	0.0644	0.1779	0.0260	0.0658	0.0296	0.0176	0.0222	0.0206

0.065 cm^2 cm^{-2}. The lowest DIVEp was observed in the Bt horizon, 0.0176 cm^2 cm^{-2}, and the other horizons showed DIVEp of ca. 0.02–0.03 cm^2 cm^{-2}.

3.6. Water retention and hydraulic conductivity

Interpolated SWRCs are shown in Fig. 4a and water retention parameters obtained via the RETC programme from measured data are presented in Table 2. Owing to the fact that the coefficients of regression of observed vs. fitted values (R^2) were in the range of 0.991–1.000, it was possible to obtain an accurate prediction of soil hydraulic properties. Within the soil water potential range of −30 to −0.01 kPa (volume of macropores, MA, equivalent to gravitational water capacity), three distinct SWRC groups were identified: representing the O and Ah horizons, the AE horizon and the remaining horizons. The observed similari-

ties in these clusters were due to similarities in structure type and degree of aggregate development, as characterised in detail in previous sections. Additionally, the previous sections had described the trends in the Retisol's pedon with regard to the mesopore volume (ME), representing the volumetric retention of water available for plants, and the micropore volume (MI), i.e. the volumetric retention of unavailable water. The maximum water capacity (MWC) was the highest in the O and Ah horizons (ca. 0.67 cm^3 cm^{-3}), decreased by ca. 27% in AE and reached ca. 0.44 cm^3 cm^{-3} in the rest of the pedon (Table 1).

Hydraulic conductivities (Ks, Fig. 4b) were classified as very high in the O horizon, high in Ah, low in AE and very low in the remaining horizons. The unsaturated hydraulic conductivity (K) decreased with decreasing effective saturation (ES), calculated as ES = (WC − RWC)/(MWC − RWC), most rapidly in the surface soil layer. The decrease was slower in the Ah horizon. For the
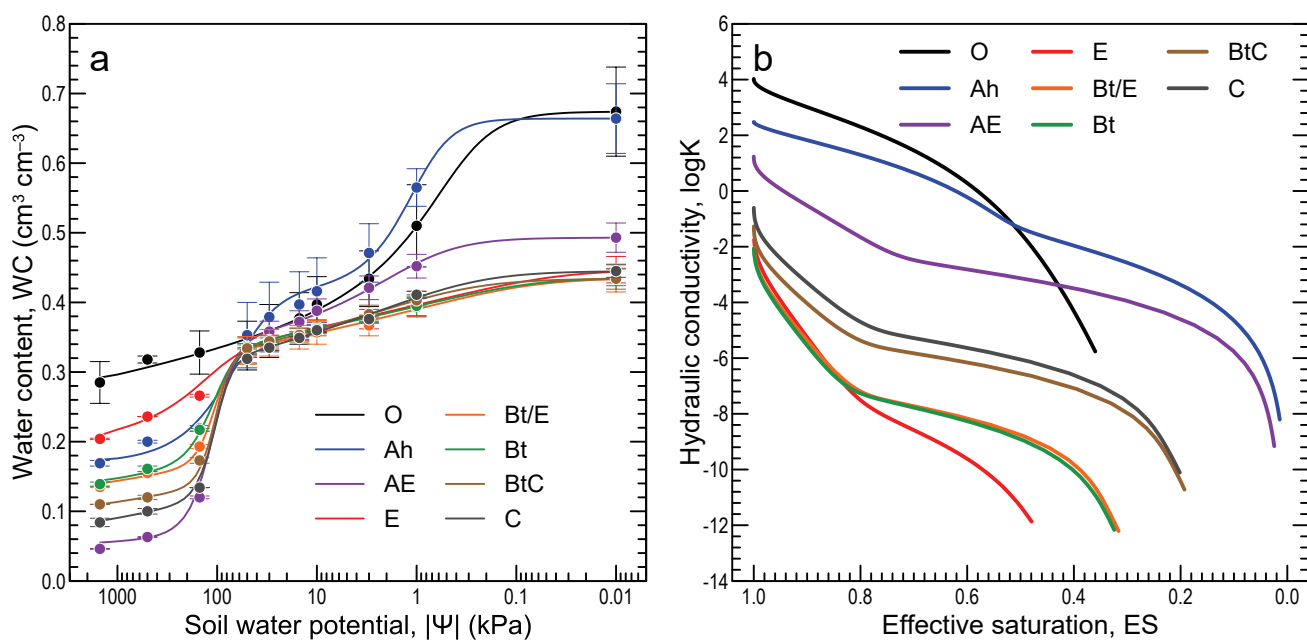
Fig. 4. (a) Observed (dots) and fitted (lines) soil water retention curves; (b) hydraulic conductivity vs. effective saturation in the Retisol's horizons.

9

other horizons, the strongest decline of K was noted in the ca. 0.8–1 saturation range. Once this ES value was reached, K decreased at a much slower rate. The shapes of the plots for the BtC and C horizons and also Bt/E and Bt horizons were similar.

Figs. 5 and 6 present fluxes (Fig. 5a) and effective saturation with water (ES) and water content (WC) at the selected depths in the Retisol's pedon (Figs. 5b, c) and on selected days (Figs. 6a, b) during a month of simulated precipitation. It is evident that the largest changes in WC occurred in the upper part of the pedon (O–E), with stable WC and ES starting from 54 cm downwards (Figs. 5 and 6). The initially unsaturated soil (Fig. 5; day 0, ES in the range 0.5–0.8) was wetted via precipitation occurring irregularly during 31 days. The precipitation induced a downward flux mostly affecting the O–E horizons. Characteristic changes in ES

and WC in the upper part of the Retisol's pedon were observed on days 4 and 25. After four days of precipitation, soil absorbed 4.24 cm of water. At depths of 0 and 8 cm, the soil did not completely saturate (ES of 0.64 and 0.74, respectively), but owing to a sufficient hydraulic conductivity K of ca. 7 cm d^{-1} (Fig. 4b) and some water present in macropores (i.e. ES exceeding 0.531 and 0.499, respectively), a downward flux appeared supplying the lower layers with water. Consequently, rapid soil wetting occurred at depths of 18 cm and especially 38 cm, leading to (almost) full saturation (specifically with ES above 0.765 and 0.814, respectively) and a vertical water flux (Fig. 5). The water drainage resulted in a WC decrease at the depths of 0, 8, 18 and 38 cm. During the following days, the upper 18 cm of the pedon displayed recurring increases in WC and ES after rainfall followed
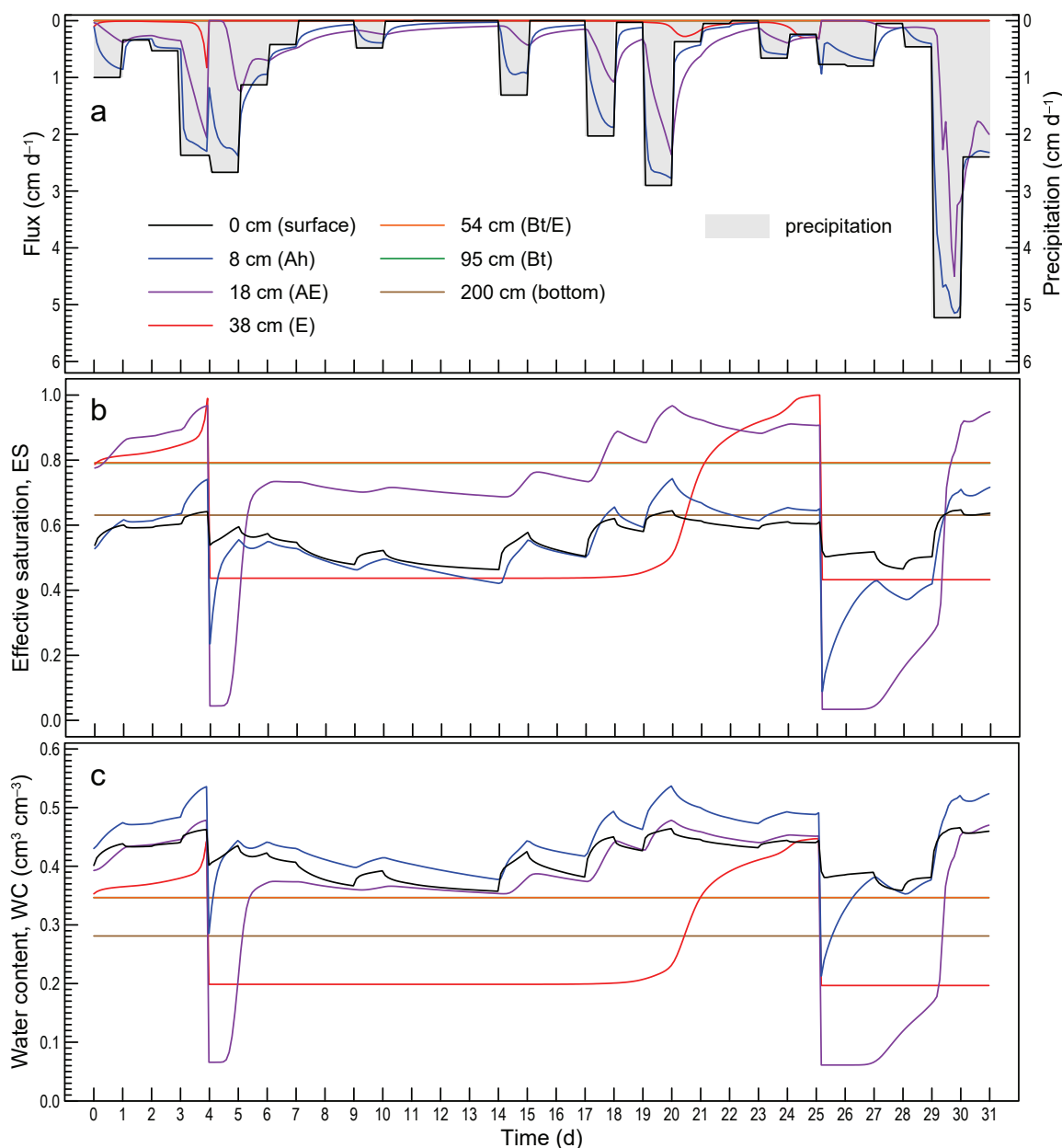
Fig. 5. (a) Flux (left axis) and precipitation (right axis), (b) effective saturation and (c) water content at selected depths of the Retisol's pedon during a month of simulated precipitation.
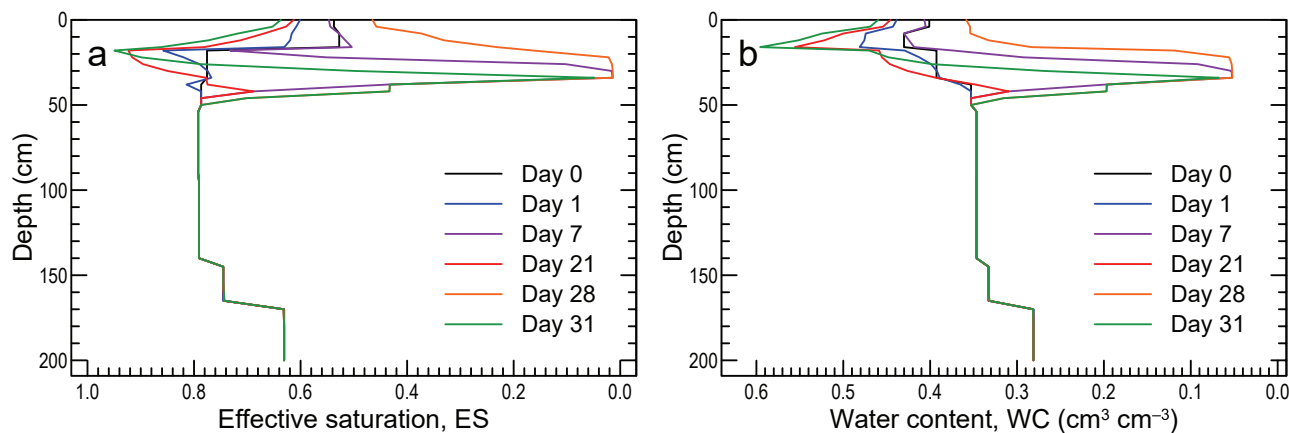
Fig. 6. (a) Effective saturation and (b) water content in the Retisol's pedon before (Day 0) and on chosen days of a month of simulated precipitation.

by respective decreases, indicating a slow downward movement of water. These fluxes gradually recharged underlying soil layers, hence an increase in ES was detected at a depth of 38 cm after day 17, with a further ES growth following rainfall. As a result, after day 25, the changes in WC and ES resembled those observed on day 4. Under the chosen time span and boundary conditions of the simulation, which took into account Ks measured for the Retisol's horizons, virtually no changes in WC and ES were detected at depths of 54, 95 and 200 cm (Figs. 5 and 6).

3.7. Relationships among the studied parameters

The relationships among the studied parameters were verified using PCA (Fig. 7) and a subsequent analysis of Pearson's linear correlations (Table 4). The PCA model explained 89.61% of the data variation with the first two principal components (PC1 and PC2). PC1 covered 67.28% of the variance and was controlled by the majority of variables: LA, AA, MA, PD, AAp5, logKs, BD, NAs, TP, TOC, ANp, ELG1p and Ks which were in gen-

eral negatively correlated with PC1. PC2 explained 22.33% of the variance, with the most important variables being AAp2, AAp1, NAp and ME. Other variables (MI, ANs, AAp3, DIVEp, AAp4) had smaller contributions in either PC1 or PC2 which was clear by the shorter length of the relevant vectors in relation to the correlation ellipse (Fig. 7, top and right axis, green ellipse). The plot for the variable loadings revealed their correlation structure, i.e. grouping of variables. This indicated the relationships between the morphometric parameters and the physicochemical properties of the soil. Consequently, image analysis of soil structure could support the interpretation of soil hydraulic properties. The score component of the biplot (Fig. 7, bottom and left axis) revealed four groups of soil horizons: O, Ah, AE and E–C, with E to some degree separated from the last group. Dots representing specific horizons were located near the vectors of variables (the Retisol's properties) which achieved the highest values in these horizons. The linear correlation coefficients (Table 4) quantitatively indicated the strength of relationships among the parameters studied and confirmed the patterns revealed via PCA.
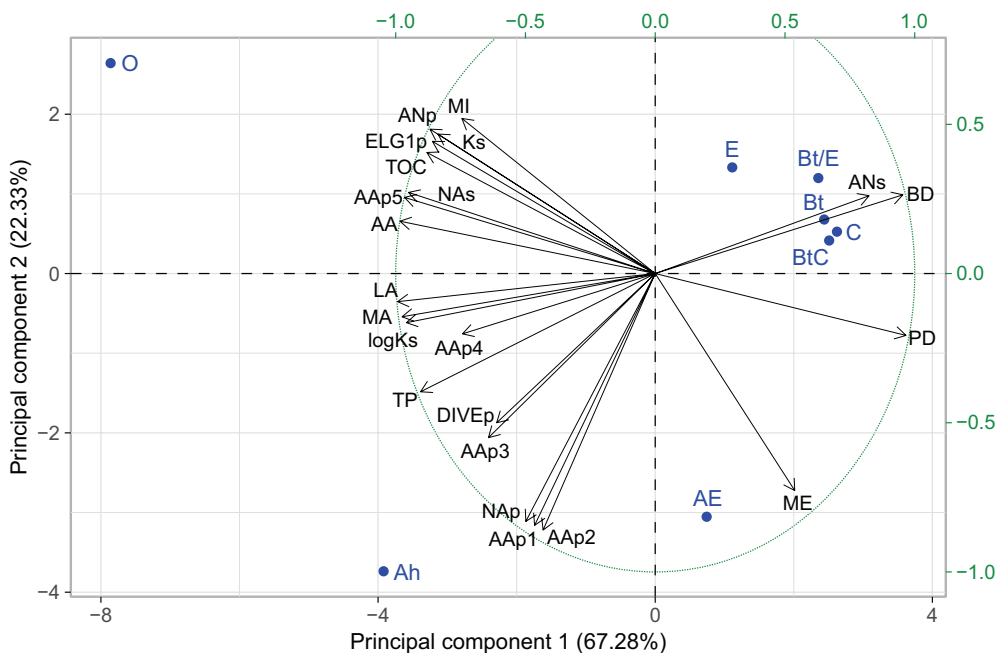
Fig. 7. Principal component analysis (PCA) for the Retisol's horizons. Biplot features: the Retisol's horizons – bottom and left axis showing PC1 and PC2 score, respectively; parameters – top and right axis showing loadings on PC1 and PC2, respectively.

11

Table 4.
Pearson's correlation coefficients for selected parameters.

	AA	AAp1	AAp2	AAp4	AAp5	LA	NAs	ANp	ELG1p	PD	BD	TP	TOC	MI	MA
AAp2		0.986	–												
AAp5	0.997				–										
LA	0.962				0.938	–									
NAp		0.997	0.992												
NAs	0.988				0.994	0.929	–								
ANp	0.940				0.964		0.961	–							
ELG1p	0.930				0.952		0.973	0.974	–						
DIVEp				0.939											
PD	−0.992				−0.992	−0.951	−0.997	−0.942	−0.956	–					
BD					−0.975						–				
TP					0.935						−0.989	–			
TOC	0.945				0.963		0.983	0.972	0.998	−0.970			–		
ME														−0.957	
MA	0.935				0.906	0.979				−0.912	−0.983	0.959			–
Ks	0.914				0.938		0.963	0.968	0.999	−0.945			0.996		
logKs	0.920					0.977				−0.913	−0.966	0.934			0.948

4. Discussion

Forest soils are characterised by a specific structure. In natural or minimally anthropogenically influenced forest soils, the arrangement of genetic horizons within the pedon remains undisturbed. The top layer is the organic horizon, with genetic horizons beneath resulting from long-term pedogenesis without anthropogenic pressure. The continuous deposition of organic matter on the forest floor leads to the formation of organic horizons. The loss of organic matter during forest management is relatively minimal. In addition, organic matter does not rapidly oxidise owing to the cool, humid and shaded conditions of the forest floor. The presence of an organic layer and an intact sequence of genetic horizons distinguish natural forest soils from arable or anthropogenic ones (e.g. Domżał et al., 1993). The structure of the forest soil is intrinsically linked to the nature of the forest ecosystem with its soil fauna which induces significant and beneficial changes in soil structure. The vegetation and organic layer protect the surface of forest soils from the destructive effects of heavy rainfall. A characteristic feature of forest soils is also the abundance of roots which typically extend to considerable depths. These factors contribute to the development of distinctive types of structure in forest soils (e.g. Carmean, 1957; Boyle, 2005).

To enhance the current knowledge of forest soils, this paper provides a unique and comprehensive description of the physical state of a forest Retisol, including morphometric parameters of the structure, as well as selected physicochemical characteristics of the identified genetic horizons, ranging from the organic horizon to the parent material. The analysis of the Retisol's structure distinguished three zones with dissimilar properties within the studied pedon: the organic layer and the mineral material in which the Ah horizon was differentiated from the rest of the pedon. The size distributions of pore and solid phase element

cross-sections clearly reflected the structural features visible in the images (Bryk, 2010). In the organic horizon, solid phase elements such as plant residues were separated and loosely arranged and the soil pores were significantly interconnected (Fig. 2). As a result, the pore size distributions were initially rather flat, up to the equivalent diameter of 3 mm, due to the low volume of small pore cross-sections, and then increased visibly, illustrating the presence of a continuous and large pore space (Fig. 3). The solid phase, on the other hand, consisted of discrete elements (aggregates) of varying dimensions (Figs. 2 and 3). In the Ah horizon, there was a marked decrease in the volume of pores > 3 mm and at the same time an increase in the amount of large solid phase elements > 30 mm at the expense of smaller elements. In the remaining mineral part of the pedon (AE–C), pores of various sizes were observed, with a predominance of those smaller than 3 mm. The solid phase was generally continuous, as evidenced by the predominance of elements > 30 mm.

These findings were further supported by the morphometric parameters (Bryk, 2008). The porosity measured by image analysis (AA) accurately described the state of soil structure. Together with the relative length of the boundary between pore and solid phase element cross-sections (LA), the relative number of pore and solid phase element cross-sections (NAp and NAs, respectively) and the mean area of pore and solid phase element cross-section (ANp and ANs, respectively), allowed an in-depth quantitative analysis of soil structure types (Słowińska-Jurkiewicz et al. 2004). The organic horizon exhibited very high porosity and the relative length of the boundary between pore and solid phase element cross-sections, as well as large mean area and medium relative number of pore cross-sections and very small area and very high relative number of solid phase element cross-section. These features were indicative of a loose arrangement of the soil. The mineral soil horizon with aggregate structure (Ah) revealed medium porosity and relative length of the

pore-solid phase boundary. The relative number of pore cross-sections was high and solid phase element low, with their mean area very small and small, respectively. The mineral horizons (E, Bt/E, Bt, BtC and C) that were not aggregated showed a very low porosity, relative length of the pore-solid phase boundary, relative number of solid phase elements and mean area of pore cross-sections. The relative number of pore cross-sections was low or very low, while the mean area of solid phase elements was medium or large. The AE horizon had zones of both aggregate and non-aggregate structure, with most of the morphometric parameters being similar to those in the underlying horizons. Similar results with respect to macrostructure were obtained by Sauzet et al. (2016) for a forest Luvisol developed in decarbonated Quaternary loess deposits (France). During a field survey of a soil profile, they found a moderately-developed medium-sized granular structure in the A horizon, a weakly-developed fine subangular blocky structure in E, a weakly- or moderately-developed coarse or medium prismatic aggregates in the Bt horizon and a massive structure in the parent material. This description indicated the presence of pores–planes in horizons E and B. Kabała et al. (2019) recognised qualitatively analogous structure types in forest Luvisols and Retisols developed from thick loess sediments (Poland). It can therefore be concluded that the Retisol analysed in the current study had a structure typical of a silt loam clay-illuvial soil, commonly observed under long-standing forests.

The lower compactness in the upper part of the Retisol was validated by the higher total porosity (TP) which gradually decreased with depth, in line with the values of the relative length of the pore-solid phase boundary (Table 4). This relationship was reversed for the bulk density (BD), as total porosity and bulk density are negatively correlated (for the studied Retisol, R = −0.989). The recorded bulk density values were consistent with previous results for forest Luvisols or Retisols developed from loess (Brahy et al., 2000; Kabała et al., 2019; Sauzet et al., 2016).

Additionally, a decrease in the particle density (PD) corresponded to an increase in the porosity, relative length of the pore-solid phase boundary, volume of the pores > 3 mm (AAp5), mean area of pore cross-section and the relative number of solid phase element cross-sections. A decrease in particle density in the soil is typically linked to an increase in organic matter content. It was also confirmed in the present study, because the correlation coefficient between the particle density and the total organic carbon (TOC) was −0.970. Thus, the abovementioned morphometric parameters increased with the increasing carbon content, indicating the formation and development of an aggregate structure favoured by the soil organic matter (humus). Firstly, organic matter is a source of nutrients for soil fauna. Soil organisms create wide pores (channels) through their activity, which become the main paths for water and air movement, thus increasing the biologically active volume of the soil. In addition, the soil fauna efficiently mixes organic and mineral materials and creates water-stable casts. Secondly, organic matter functions as a binder for soil particles, thus promoting the formation and stability of soil aggregates (Cosentino et al., 2006; Morris, 2004; Słowińska-Jurkiewicz et al., 2013).

Water retention depends in a complex way on soil structure and composition, consequently the shapes of the soil water retention curves (SWRCs) reflected the effect of pedogenic processes on the hydraulic properties of the Retisol's horizons. Glina et al. (2014) also indicated a similar relationship when comparing SWRCs in the Ψ range from 0 to −50 kPa of homogeneous and lamellic illuvial horizons of Luvisols developed from loess.

For the Retisol, the SWRCs shapes as characterised by the macro-, meso- and micropore volume (MA, ME and MI, respectively) did not show a statistically confirmed correlation with TOC. Organic matter, however, influenced the Retisol's structure, i.e. the size, number and arrangement of soil pores and solid phase elements, which in turn modelled the water retention functions. Similarly, Toková et al. (2023) found a reduction in bulk density and an increase in total porosity of an arable silty loam Haplic Luvisol under repeated biochar application at a dose of 20 t ha^{-1}, which improved the saturated hydraulic conductivity, water storage and overall hydrological soil balance. Typically, the content of organic matter (organic carbon) is among the most important input parameters for predicting soil hydraulic properties. According to Tóth et al. (2015), texture in combination with the organic carbon content provided an adequate basis for the prediction of soil water status in most cases. However, the effect of organic matter on water retention and hydraulic conductivity is often inconclusive, since it indirectly impacts hydraulic properties through soil structure (Rawls et al., 2003; Lado et al., 2004; Nemes et al., 2005; Saxton and Rawls, 2006; Tóth et al., 2015).

In the current study, the O, Ah and AE horizons were distinct from the rest of the pedon, showing a predominance of macropores based on the SWRC measurements. This undoubtedly resulted also in higher saturated and unsaturated hydraulic conductivities (Ks and K) in these horizons relative to the rest of the pedon. Recent studies by Zvala et al. (2020) indicated that saturated hydraulic conductivity could be very high in the forest floor, particularly in the loose litter layer typical of rich deciduous forests. The authors further emphasised that saturated hydraulic conductivity decreased in the organic horizon from top to bottom, with increasing decomposition and aggregation of organic material. However, in the current study, due to the relatively low thickness of the O horizon, no such trend was observed.

The saturated hydraulic conductivity decreased downwards the Retisol's pedon with decreasing organic carbon (R = 0.996) and increasing particle density (R = −0.945). Plots of unsaturated hydraulic conductivity (Fig. 4b) indicated comparable shapes between the BtC and C horizons, as well as the Bt/E and Bt horizons, owing to their similar structure.

The analysis of the shape and orientation of soil pore cross-sections showed that ca. 14% (O) and 60–84% (Ah–C) of the volume of pores > 100 pix^2 were elongated, with 76% (C) and 83–88% (O–BtC) of those being vertical and diagonal pores. The Retisol's horizons revealed comparable proportions of diagonal with vertical pore cross-sections (DIVEp), although their volumes varied between 0.02–0.18 cm^2 cm^{-2}. No defined effect of the amount of these pores on the saturated hydraulic conductivity was observed. It depended primarily on the porosity and the vol-

13

ume of the largest pores (> 3 mm) and increased with increasing number of solid phase elements and mean area of pore cross-section, i.e. it was larger for aggregate structures (Table 4). In this context, the strong positive relationship (R = 0.999) between the saturated hydraulic conductivity and the volume of non-elongated (round) pore cross-sections (ELGp1) may therefore seem unexpected, since the round pores were usually isolated in soil structure images. Indeed, most of the round pore cross-sections in the deeper horizons of the Retisol were small and isolated (e.g. *Nadelstichporen*), so they did not support the water movement. Nevertheless, the soil also contained numerous large biopores (channels) that were perpendicular to the cutting plane and thus detected by image analysis as round objects. These pores undoubtedly sustained the water flow. It can be assumed that the Ks–ELGp1 relationship indicated a general tendency for the hydraulic conductivity to increase with growing pore volume, as the round pores accounted for ca. 86% (O-A) and 16–40% (A–C) of the volume of the pores > 100 pix^2 and the volume of round pores correlated positively with the porosity (R = 0.930).

The Retisol was situated atop a hill, in an area of undulating (hilly) relief. The modelling of water content over the 31-day period showed that the soil had a favourable (balanced) water-air regime and an adequate water content. Due to the poorly permeable layers present in the pedon (Bt/E, Bt), this soil can experience periodic water accumulation in the spring and autumn, as well as occasionally in the peak growing season. However, neither waterlogging nor gleyic properties were observed in the field. Considering the recognised soil structure, the downward flow of water into the pedon may be slow, but it is still possible owing to the zones of an aggregate structure and random wide pores, both resulting from bioturbation which locally loosened the soil in the Bt/E, Bt, BtC and C horizons. A similar effect was recently reported by Sauzet et al. (2021) who determined the arrangement of earthworm channels in a laboratory experiment on an arable Luvisol of a silt loam texture (France). They stated that earthworms opened some large connected biopores in repacked soil columns, allowing for rapid air and water flows.

5. Conclusions

The resin-impregnated blocks allowed for a morphographic, morphological and morphometric evaluation of the structure of the entire Retisol's pedon from the organic horizon to the parent material. The field survey and the soil structure images indicated that the studied forest soil had an undisturbed sequence of genetic horizons. The soil flora and fauna played an important and distinctive role in shaping the soil structure, causing bioturbation.

The morphometric parameters provided a quantitative and synthesised assessment of the structure in the Retisol's pedon. This enabled the identification of the characteristic structural features in the O, Ah, AE, E, Bt/E, Bt, BtC and C genetic horizons.

The qualitative and quantitative analysis of the structure revealed that the organic horizon had a loose arrangement, Ah had an aggregate structure, AE had zones of an aggregate and non-aggregate structure, while the remaining mineral horizons showed essentially a non-aggregate structure with varying proportions and sizes of planes and biogenic pores. The round pore cross-sections prevailed in the organic horizon, whereas the elongated pore cross-sections predominated in mineral horizons. The vertical and diagonal pores accounted for more than 76% of the elongated pores.

Both the morphometric and selected physicochemical parameters were studied, facilitating the detailed analysis of the Retisol's physical state. Numerous positive correlations were found among the morphometric parameters: AA, AAp1, AAp2, AAp4, AAp5, LA, NAp, NAs, ANp, ELGp1 and DIVEp. Positive correlations were found for TOC and Ks with AA, AAp5, NAs, ANp and ELGp1; logKs with AA and AAp5; MA with AA, AAp5, LA; logKs with TP and MA. Negative correlations were detected for PD with AA, AAp5, LA, NAs, ANp and ELGp1; BD with LA; Ks with PD; logKs with PD and BD.

The Retisol's structure type and degree of aggregate development directly influenced its hydraulic conductivity and retention capacity. The O and Ah horizons had the highest MWC, MA and Ks. Intermediate values of these parameters were noted in the AE horizon and lower – in the remaining of the pedon. In the 31-day experiment modelling fluctuating precipitation, the soil water content and effective saturation varied mainly in the upper part of the pedon (the O–E horizons). Under the chosen time span and boundary conditions, virtually no changes in these parameters were observed at lower depths (the Bt–C horizons).

The research resulted in a comprehensive set of physicochemical and morphometric parameters along with structure images that were unavailable in other studies, covering the physical state of the entire forest Retisol's pedon. The results obtained may serve, for example, as a reference (control) for analogous soils located in non-forest ecosystems and become an element in space-for-time substitution scenarios aimed at assessing the intensity of anthropogenic transformation.

Acknowledgments

References

Aguilar, J., Dorronsoro-Fdez, C., Fernández, J., Dorronsoro Diaz, C., Martin, F., Dorronsoro, B., 2023. Soil microscopy. Soil Micromorphography. Interactive Multimedia Programme for Self-studying Soil Thin Section Description (http://edafologia.ugr.es/micgraf/indexw.htm (accessed on 15.03.2023)).

Beck, H., Zimmermann, N., McVicar, T., Vergopolan, N., Berg, A., Wood, E.F., 2018. Present and future Köppen-Geiger climate classification maps at 1-km resolution. Scientific Data 5, 180214. https://doi.org/10.1038/sdata.2018.214

Beckmann, W., Geyger, E., 1967. Entwurf einer Ordnung der natürlichen Hohlraum-, Aggregat-, und Strukturformen in Boden. [In:] Kubiëna, W.L. (Ed.), Die mikromorphometrische Bodenanalyse. Ferdinand Enke Verlag, Stuttgart, 163–188.

Benjamini, Y., Hochberg, Y., 1995. Controlling the false discovery rate: a practical and powerful approach to multiple testing. Journal of the Royal Statistical Society Series B 57, 289–300. https://doi.org/10.1111/j.2517-6161.1995.tb02031.x

Boyle, J.R., 2005. Forest soils. [In:] Hillel, D. (Ed.) Encyclopedia of Soils in the Environment. Elsevier, 73–79. https://doi.org/10.1016/B0-12-348530-4/00033-3

Brahy, V., Deckers, J., Delvaux, B., 2000. Estimation of soil weathering stage and acid neutralizing capacity in a toposequence Luvisol–Cambisol on loess under deciduous forest in Belgium. Europen Journal of Soil Science 51(1), 1–13. https://doi.org/10.1046/j.1365-2389.2000.00285.x

Brewer, R., Sleeman, J.R., 1960. Soil structure and fabric. Their definition and description. Journal of Soil Science 11, 172–185. https://doi.org/10.1111/j.1365-2389.1960.tb02213.x

Bryk M., 2008. Morphometric evaluation of transformation of soil structure from coherent into aggregate one. Acta Agrophysica 12(3), 595–606.

Bryk M., 2010. Changes of size distribution of macropores and solid phase elements in Rendzic Leptosol caused by tillage. Acta Agrophysica 15(2), 221–232.

Bryk, M., 2016. Macrostructure of diagnostic B horizons relative to underlying BC and C horizons in Podzols, Luvisol, Cambisol, and Arenosol evaluated by image analysis. Geoderma 263, 86–103. https://doi.org/10.1016/j.geoderma.2015.09.014.

Bryk, M., Kołodziej, B., 2014. Assessment of water and air permeability of chernozem supported by image analysis. Soil and Tillage Research 138, 73–84. https://doi.org/10.1016/j.still.2013.12.008

Bryk, M., Słowińska-Jurkiewicz, A., Kołodziej, B., 2005. Changes of pore orientation in soil lessivé caused by tillage measures. Annales UMCS Sectio E Agricultura 60, 229–236.

Buraczyński, J. (Ed.), 2002. Roztocze. Natural environment. Wydawnictwo Lubelskie, Lublin.

Carmean, W.H., 1957. The structure of forest soils. Ohio Journal of Science 57(3), 165–168.

Cosentino, D., Chenu, C., Le Bissonnais, Y., 2006. Aggregate stability and microbial community dynamics under drying–wetting cycles in a silt loam soil. Soil Biology and Biochemistry 38(8), 2053–2062. https://doi.org/10.1016/j.soilbio.2005.12.022

Domżał, H., Hodara, J., Słowińska-Jurkiewicz, A., Turski, R., 1993. The effects of agricultural use on the structure and physical properties of three soil types. Soil and Tillage Research 27(1–4), 365–382. https://doi.org/10.1016/0167-1987(93)90078-4

Durner, W., 1994. Hydraulic conductivity estimation for soils with heterogeneous pore structure. Water Resources Research 30(2), 211–223. https://doi.org/10.1029/93WR02676

FitzPatrick, E.A., 1984. Micromorphology of Soils. Chapman and Hall, London, New York.

Fox, J., Weisberg, S., 2019. An {R} Companion to Applied Regression, Third Edition. Thousand Oaks (CA), Sage. https://socialsciences.mcmaster.ca/jfox/Books/Companion/

Gilewska, S., 1999. Poland's natural environment in comparison with Europe. [In:] Starkel, L. (Ed.), Geography of Poland. Natural environment. Wydawnictwo Naukowe PWN, Warszawa, 15–24.

Glina, B., Jezierski, P., Kabała, C., 2013. Physical and water properties of Albeluvisols in the Silesian Lowland (SW Poland). Soil Science Annual 64(4), 123–129. https://doi.org/10.2478/ssa-2013-0019

Glina, B., Waroszewski, J., Kabała, C., 2014. Water retention of the loess-derived Luvisols with lamellic illuvial horizon in the Trzebnica Hills (SW Poland). Soil Science Annual 65(1), 18–24. https://doi.org/10.2478/ssa-2014-0003

Huang, X., Horn, R., Ren, T., 2022. Soil structure effects on deformation, pore water pressure, and consequences for air permeability during compaction and subsequent shearing. Geoderma 406, 115452. https://doi.org/10.1016/j.geoderma.2021.115452

IMGW–PIB, 2023. Available online: https://danepubliczne.imgw.pl/data/dane_pomiarowo_obserwacyjne/dane_meteorologiczne/dobowe/opad/2011/2011_07_o.zip (accessed on 28 April 2023).

ISO 10390, 2021. Soil, treated biowaste and sludge – Determination of pH.

ISO 10693, 1995. Soil quality – Determination of carbonate content – Volumetric method.

ISO 11277, 2009. Soil quality – Determination of particle size distribution in mineral soil material – Method by sieving and sedimentation.

ISO 11508, 2017. Soil quality – Determination of particle density.

ISO 14235, 1998. Soil quality – Determination of organic carbon by sulfochromic oxidation.

IUSS Working Group WRB, 2022. World Reference Base for Soil Resources. International soil classification system for naming soils and creating legends for soil maps. 4th edition. International Union of Soil Sciences (IUSS), Vienna, Austria.

Jongerius, A., Rutherford, G.K. (Eds.), 1979. Glossary of Soil Micromorphology. Centre for Agricultural Publishing and Documentation, Wageningen.

Kabała, C., Musztyfaga, E., 2015. Clay-illuvial soils in the Polish and international soil classifications. Soil Science Annual 66(4), 204–213. https://doi.org/10.1515/ssa-2015-0038

Kabała, C., Przybył, A., Krupski, M., Łabaz, B., Waroszewski, J., 2019. Origin, age and transformation of Chernozems in northern Central Europe – New data from Neolithic earthen barrows in SW Poland. Catena 180, 83–102. https://doi.org/10.1016/j.catena.2019.04.014

Kassambara, A., Mundt, F., 2020. factoextra: Extract and Visualize the Results of Multivariate Data Analyses. R package version 1.0.7, https://CRAN.R-project.org/package=factoextra

Klíč, R., Kravka, M., Wimmerová, L., Viruez, J.L.G., Válová, M., Miháliková, M., 2022. Microplastics locked in water-stable aggregates of the Haplic Luvisol and role of land use on their potential mobility. Water, Air, and Soil Pollution 233, 37. https://doi.org/10.1007/s11270-022-05499-8

Kołodziej, B., Bryk, M., Słowińska-Jurkiewicz, A., 2004. Use of pore elongation index for structure evaluation of soil lessivé affected by tillage measures. Annales UMCS Sectio E Agricultura 59(1), 337–343.

Krupski, M., Mackiewicz, M., Kabała, C., Ehlert, M., Cendrowska, M., 2021. Earthen mounds in the Głubczyce Forest (SW Poland) – are they prehistoric long-barrows? Geoarchaeology of the Silesian soil record and human-environment interplay in the Holocene. Praehistorische Zeitschrift 96(2), 413–433. https://doi.org/10.1515/pz-2021-0004

Lado, M., Paz, A., Ben-Hur, M., 2004. Organic matter and aggregate-size interactions in saturated hydraulic conductivity. Soil Science Society of America Journal 68, 234–242. https://doi.org/10.2136/sssaj2004.2340

Le, S., Josse, J., Husson, F., 2008. FactoMineR: An R Package for Multivariate Analysis. Journal of Statistical Software 25(1), 1–18. https://doi.org/10.18637/jss.v025.i01

Morris, L.A., 2004. Soil organic matter forms and functions. [In:] Burley, J., Evans, J., Youngquist, J.A. (Eds.) Encyclopedia of Forest Sciences, Elsevier, Oxford, 1201–1207.

Nemes, A., Rawls, W.J., Pachepsky, Y.A., 2005. Influence of organic matter on the estimation of saturated hydraulic conductivity. Soil Science Society of America Journal 69, 1330–1337. https://doi.org/10.2136/sssaj2004.0055

Obalum, S.E., Uteau-Puschmann, D., Peth, S., 2019. Reduced tillage and compost effects on soil aggregate stability of a silt-loam Luvisol using different aggregate stability tests. Soil and Tillage Research 189, 217–228. https://doi.org/10.1016/j.still.2019.02.002

Paluszek, J., 2011. Criteria of evaluation of physical quality of Polish arable soils. Acta Agrophysica 191, 1–139.

Polish Soil Classification, 2019. Soil Science Society of Poland, Commission on Soil Genesis, Classification and Cartography. Wydawnictwo

Uniwersytetu Przyrodniczego we Wrocławiu, Polskie Towarzystwo Gleboznawcze, Wrocław –Warszawa, 235 pp.

R Core Team, 2022. R: A language and environment for statistical computing. R Foundation for Statistical Computing, Vienna, Austria. https://www.R-project.org/

Rawls, W.J., Pachepsky, Y.A., Ritchie, J.C., Sobecki, T.M., Bloodworth, H., 2003. Effect of soil organic carbon on soil water retention. Geoderma 116(1–2), 61–76. https://doi.org/10.1016/S0016-7061(03)00094-6

Russ, J.C., Dehoff, R.T., 2000. Practical Stereology, 2nd ed. Kluwer Academic/Plenum Publishers, New York, NY.

Sauzet, O., Cammas, C., Barbillon, P., Étienne, M-P., Montagne, D., 2016. Illuviation intensity and land use change: Quantification via micromorphological analysis. Geoderma 266, 46–57. https://doi.org/10.1016/j.geoderma.2015.11.035

Sauzet, O., Kohler-Milleret, R., Füllemann, F., Capowiez, Y., Boivin, P., 2021. *Nicodrilus nocturnus* and *Allolobophora icterica* drill compacted soils but do not decrease their bulk density – A laboratory experiment using two contrasted soils at two different compaction levels. Geoderma 402, 115164. https://doi.org/10.1016/j.geoderma.2021.115164

Saxton, K.E., Rawls, W.J., 2006. Soil water characteristic estimates by texture and organic matter for hydrologic solutions. Soil Science Society of America Journal 70, 1569–1578. https://doi.org/10.2136/sssaj2005.0117

Šimůnek, J., Huang, K., van Genuchten, M.T., 1998. The HYDRUS code for simulating the one-dimensional movement of water, heat, and multiple solutes in variably-saturated media. Version 6.0. Res. Rep. 144. U.S. Salinity Laboratory, Riverside (CA), USA.

Šimůnek, J., Šejna, M., Saito, H., Sakai, M., van Genuchten, M.T., 2018. The HYDRUS-1D Software Package for Simulating the One-Dimensional Movement of Water, Heat, and Multiple Solutes in Variably-Saturated Media. Manual, version 4.17. Department of Environmental Sciences, University of California, Riverside (CA), USA, 348 pp.

Słowińska-Jurkiewicz A., Kołodziej B., Bryk M., 2004. Effect of tillage measures on structure of the soil lessivé – morphometrical evaluation of macropores. Annales UMCS Sectio E Agricultura 59(1), 329–335.

Słowińska-Jurkiewicz, A. 1989. Structure, water and air properties of soils developed from loess. Polish Agricultural Annuals Series D Monographs, 218, 76 pp.

Słowińska-Jurkiewicz, A., Bryk, M., Kołodziej, B., Jaroszuk-Sierocińska, M., 2012. Makrostruktura gleb Polski – Macrostructure of soils in Poland. AWR Magic, Lublin, Poland. https://hdl.handle.net/20.500.12838/bd3aec92-da78-4e7b-bf33-62a9d7a5b0ba

Słowińska-Jurkiewicz, A., Bryk, M., Medvedev, V.V., 2013. Long-term organic fertilization effect on chernozem structure. International Agrophysics 27(1), 81–87. https://doi.org/10.2478/v10247-012-0071-1

Soil Atlas of Europe, 2005. European Soil Bureau Network, European Commission, Office for Official Publications of the European Communities, L-2995 Luxembourg, 128 pp.

Solon, J. et al., 2018. Physico-geographical mesoregions of Poland: Verification and adjustment of boundaries on the basis of contemporary spatial data. Geographia Polonica 91(2), 143–170. https://doi.org/10.7163/GPol.0115

Święcicki, C., Siuta, J., Sienkiewicz, J., Trzecki, S., Kiersnowski, J., 1972. Selected soil properties influencing the conditions of agricultural engineering development. Zeszyty Problemowe Postępów Nauk Rolniczych – Advances of Agricultural Sciences Problem Issues, 135.

Toková, L., Igaz, D., Horák, J., Aydýn, E., 2023. Can application of biochar improve the soil water characteristics of silty loam soil? Journal of Soils and Sediments. https://doi.org/10.1007/s11368-023-03505-y

Tóth, B., Weynants, M., Nemes, A., Makó, A., Bilas, G., Tóth, G., 2015. New generation of hydraulic pedotransfer functions for Europe. European Journal of Soil Science 66(1), 226–238. https://doi.org/10.1111/ejss.12192

van Genuchten, M.T., Leij, F.J., Yates, S.R., 1991. The RETC Code for Quantifying the Hydraulic Functions of Unsaturated Soils, Version 1.0. EPA Report 600/2-91/065. U.S. Salinity Laboratory, USDA, ARS, Riverside (CA), USA.

Wągrowski, A., 1996. Detailed geological map of Poland, 859–Turobin (M-34-46-C). Polish Geological Institute, Warsaw. https://bazadata.pgi.gov.pl/data/smgp/arkusze_skany/smgp0859.jpg

Zvala, A., Orfánus, T., Čelková, A., 2020. The measurements of saturated hydraulic conductivity of the forest floor under deciduous forest. Acta Hydrologica Slovaca 21(1), 106–112. https://doi.org/10.31577/ahs-2020-0021.01.0013

Studium właściwości fizycznych leśnej gleby płowej zaciekowej wytworzonej z lessu na Wyżynie Lubelskiej, południowo-wschodnia Polska

Słowa kluczowe

Struktura gleby
Porowatość gleby
Rozkład wielkości porów
Retencja wody glebowej
Przewodnictwo wodne gleby

Streszczenie

Gleby płowe (gleby z poziomem argik), wytworzone z lessów lub innych osadów pyłowych, stanowią wysokiej jakości grunty orne ze względu na korzystne właściwości fizyczne i chemiczne. Dlatego istnieje wiele opracowań na temat takich gleb, dotyczących ich struktury, zagęszczenia, erozji, właściwości wodnych i powietrznych. Wciąż jednak brakuje ilościowych badań struktury i właściwości fizycznych analogicznych gleb leśnych. Celem niniejszych badań był kompleksowy opis właściwości fizycznych, w tym struktury, właściwości wodnych i powietrznych, leśnej gleby płowej zaciekowej wytworzonej z lessu. Wykonano analizę morfograficzną, morfologiczną i morfometryczną struktury, zbadano wybrane właściwości fizykochemiczne i wodno-powietrzne, a następnie zależności między uzyskanymi parametrami dla poziomów genetycznych O, Ah, AE, E, Bt/E, Bt, BtC i C. Badania terenowe oraz zdjęcia struktury gleby wykazały, że badana gleba leśna miała niezakłócony układ poziomów genetycznych. Struktura gleby została ukształtowana przez florę i faunę glebową powodujące bioturbacje. Jakościowa i ilościowa analiza struktury wykazała, że poziom O miał luźny układ, poziom Ah miał strukturę agregatową gruzełkową, w poziomie AE były strefy o strukturze agregatowej gruzełkowej i strukturze nieagregatowej (szczelinowej lub z kanałami), natomiast pozostałe poziomy mineralne wykazywały zasadniczo strukturę nieagregatową z różnymi udziałami i rozmiarami porów typu spękań i porów biogennych (tj. odpowiednio strukturę szczelinową lub szparkową i strukturę z kanałami). Parametry morfometryczne struktury i parametry fizykochemiczne umożliwiły szczegółową charakterystykę stanu fizycznego gleby płowej zaciekowej. Typ struktury gleby i stopień ukształtowania agregatów glebowych

miały bezpośredni wpływ na przewodnictwo wodne gleby i jej zdolność do zatrzymywania wody. Dlatego, jak wykazała symulacja opadów atmosferycznych, zawartość wody w glebie i efektywne nasycenie zmieniały się głównie w wierzchniej warstwie gleby (poziomy O-E), a praktycznie nie obserwowano takich zmian w głębszych warstwach (poziomy Bt-C). Wynikiem przeprowadzonych badań była kompleksowa analiza parametrów fizykochemicznych, morfometrycznych i zależności między nimi oraz obrazy struktury, niedostępne wcześniej w innych opracowaniach, opisujące stan fizyczny całego pedonu leśnej gleby płowej zaciekowej. Uzyskane wyniki mogą stanowić układ odniesienia (układ kontrolny) dla analogicznych gleb zlokalizowanych w ekosystemach nieleśnych. Mogą także stać się elementem badań oceniających intensywność przekształceń antropogenicznych, w których dane odnoszące się do czasu zastępuje się danymi odnoszącymi się do przestrzeni.